REMOTE FIELD INDUCED RESPONSE OF POLYMER NANOCOMPOSITES EMBEDDED WITH SURFACE-FUNCTIONALISED DIELECTRIC NANOPARTICLES

Danning Li[1,], James Barrington[2], Stephen James[2], David Ayre[1], Marcin Słoma[3], Meng-Fang Lin[4], Hamed Yazdani Nezhad[1,5,*]*

[1]Enhanced Composites and Structures Centre, School of Aerospace, Transport and Manufacturing, Cranfield University, Cranfield, UK
[2]Centre for Engineering Photonics, School of Aerospace, Transport and Manufacturing, Cranfield University, Cranfield, UK
[3]Faculty of Mechatronics, Warsaw University of Technology, Warsaw, Poland
[4]Department of Materials Engineering, Ming Chi University of Science and Technology, New Taipei, Taiwan
[5]Aeronautics and Aerospace Research Centre, Department of Mechanical Engineering and Aeronautics, City, University of London, London, UK
*Corresponding authors: danning.li@cranfield.ac.uk and hamed.yazdani@city.ac.uk

Abstract: M*atrix toughening is one of the most popular approaches to improve the overall fracture toughness of polymer composite materials. The most widely known approach for matrix toughening is the addition of a second phase such as rigid or/and rubber particles to dissipate the fracture energy, and vessels that containing healing agents that prevent further crack propagation when ruptured. Only a few studies have shown an alternative 'active toughening' by introducing an internal compressive stress field in the matrix via the mismatch in filler/matrix thermal expansion under heating. In this study, epoxy composite materials with embedded ferroelectric barium titanate nanoparticles are fabricated with the aid of silane surface functionalisation. Surface-bonded fibre grating sensors are employed to investigate the strain and temperature change of the epoxy nanocomposite materials under microwave exposure, as an attempt to introduce such field aided strain tailoring of the epoxy matrix as an active toughening mechanism.*

Keywords: Multifunctional nanocomposites; Matrix toughening; Ferroelectrics; Barium titanate; Domain wall movement

1. Introduction

High-performance composites have two major damage initiation modes when exposed to dynamic events; intra-laminar damage (e.g., matrix cracking, fibre fracture and fibre-matrix debonding) and inter-laminar damage (e.g., delamination). The intra-laminar damage is mainly dominated by matrix, fibre, and fibre-matrix interphase properties. However, it is challenging to tailor the properties of the fibre during composite's fabrication process. Therefore, the most widely adopted approach is matrix toughening owing to the diverse feasibility of its manufacturing [1]. A composite is mainly made of thermoset resins such as epoxy with a highly cross-linked structure to achieve optimal mechanical properties and thermal stability. Despite its advantageous properties, epoxy has its drawbacks of having inherent brittleness that tends to fail at relatively low fracture energy, especially under transversal direction or when subjected

to high strain rate or impact loading [2-4]. Alternatively, thermoplastic-based FRPs could hinder microcracks coalesce and growth owing to their relatively higher toughness and semi-crystalline structures in variants such as poly-ether-ether-ketone (PEEK) [5], widely used for engineering applications in the aeronautical and automotive sectors [6]. To overcome these property-driven drawbacks, numerous researches have been carried out for property enhancement via modifying epoxy with the inclusion of various micro- and nano-fillers as a second phase, such as rubber tougheners [7], silica particles [8], carbon nanoparticles [9, 10], clay [11] and others [12-16]. Although the modified epoxy with particles exhibits a promising future with excellent toughening performance, microcracks still formed in FRPs when subjected to varying or extreme operating conditions or during the manufacturing [17], indicating an inherent level of uncertainty in the material's response that will require active toughness enhancement across the material.

In this study, dielectric nanomaterials exhibiting electric field induced strain are utilized as a vision for an active toughening mechanism. Such induced strain is attributed to intrinsic mechanisms from lattice deformation and extrinsic mechanisms due to domain wall (DW) movement [18], extensively used as actuators and transducers. The inclusion of such material within a rigid epoxy materials can impose a compressive stress field in its surrounding epoxy matrix when activated its DW movements by external electric field stimulation. As result of the DW movements, a microwave stimulation at GHz frequencies induces effective dipolar displacement (leading to intrinsic strains) to the nanomaterial's molecules that, at the interface with their surrounding rigid polymer, is converted to compressive mechanical strain (Figure 1). The hypothesis of this research was based upon suggesting that microcrack propagation during dynamic and impact events would be suppressed under such microwave induced compressive field, i.e. higher strain energy would be required to create new fracture surfaces, however the current article presents attempts on the quantification of the field induced strains.

In a mono-domain ferroelectric crystal, the electric field-induced strain is generated by the intrinsic electrostriction and piezoelectric effect. In both poly-domain single crystal and polycrystalline ferroelectric materials, the domains that contain spontaneous polarisation in various directions can be aligned to the same direction by applying an external electric field. In a poly-domain ferroelectric crystal, the macroscopic strain is significantly dominated by the contribution of extrinsic strain [19]. Extrinsic effects occur at longer length-scales and the main contributor is domain wall motion, a major motivation for the hypothesis behind the development of the current research. The non-180° domain wall motion is the primary but not the only contribution of the extrinsic strain effect. Furthermore, the 90° domain wall movement also contributes to enhanced electromechanical performance in tetragonal BaTiO3 single crystals with nanodomain configurations [20, 21]. The 90° domain switching in BaTiO3 introduces a large electro-strain due to the exchange of two different crystallographic axes, and the field induced strain is one or two orders of magnitude larger than the linear electro-strain of piezoelectric materials. BaTiO3 crystals exhibit more complex domain structures due to different crystallographic axes in the tetragonal phase. Apart from the normal parallel 180° domains, there also exist adjacent domains that are polarised at 90° to each other. It is observed by Hsiang et al. [18] that the 40-80 nm BaTiO3 powders exhibit a single-domain structure while powders with sizes larger than 80 nm are polydomain tetragonal structures (the case examined by this research). Moreover, Dudhe et al. observed the 90° and 180° nano-domains of 80 nm BaTiO3 nanoparticles. Other studies focused on the polydomain structure of BaTiO3 nanoparticles with

the grain size of 50-70 nm found that the domain size is 10-12 nm [22]. In this research, polydomain BaTiO3 nanoparticles is employed to achieve the field-induced strain effect.

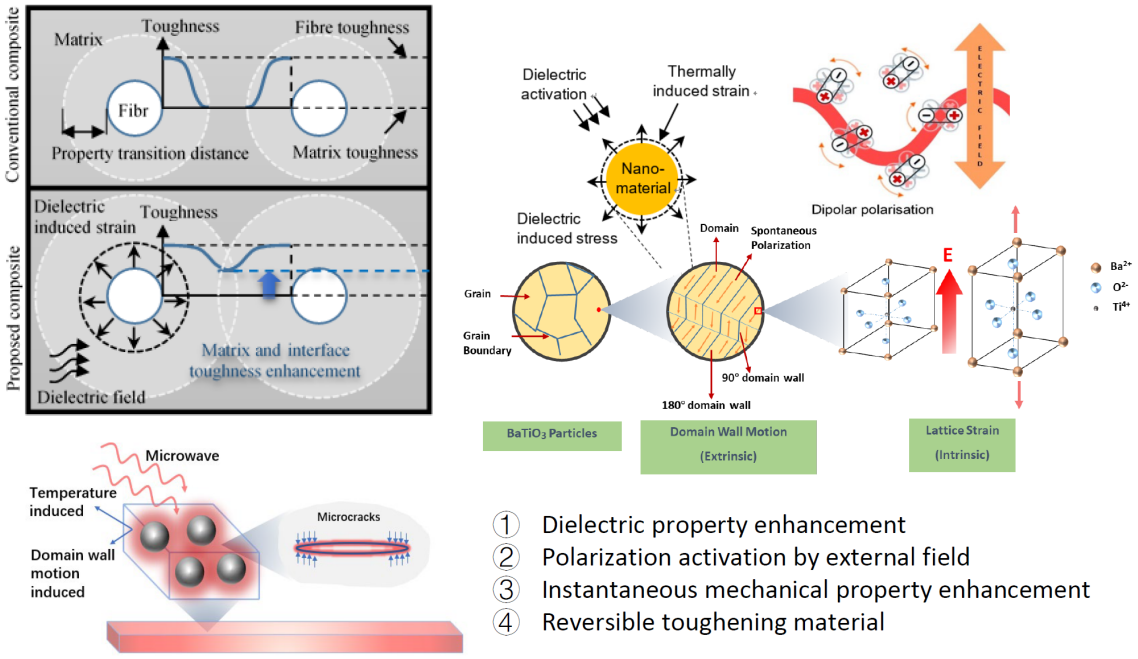

Figure 1. Schematic diagram of the extrinsic strain and intrinsic strain that contributes to macroscopic strain in a BaTiO3 particles embedded epoxy

2. Materials and Fabrication

The epoxy used in this study was Araldite LY1564, a diglycidyl ether of bisphenol A (DGEBA) and the curing agent was Aradur 3487, an amine hardener, supplied by Huntsman, UK. This epoxy resin system has relatively low viscosity and high flexibility mainly for aerospace and industrial structural composites parts. The coupling agent for surface functionalisation selected in this study was 3-glycidoxypropyl trimethoxysilane (3-GPS) supplied by Sigma-Aldrich, US. Hydrogen peroxide (H2O2, 30%) and acetic acid (C2H4O2, 99.9%) used as functionalisation aids were supplied by Sigma-Aldrich, US, and the ethanol (C2H6O, 99.9%) used for BaTiO3 dispersion by Fisher Scientific International, Inc., UK. BaTiO3 powders were supplied from Nanostructure & Amorphous Materials Inc., US. All the chemicals except BaTiO3 powders were used as received without further treatment.

The BaTiO3 powders were prepared using combustion method, therefore, firstly they were pre-treated in H2O2 for hydroxylation process to add hydroxyl group (-OH) to the surface [23]: 10g BaTiO3 nanoparticles were added into a 230mL solution of H2O2 in a round bottom flask. The mixture was then sonicated in an ultrasonic bath for 30 min and then refluxed at the boiling temperature of 30% H2O2 solution at 108°C at 100 rpm using a mechanical stirrer for six hours to facilitate the process by heating without losing H2O2. The nanoparticles were retrieved by centrifuging the resulting solution at 4500 rpm for 15 min, and washed three times with deionized water. The achieved BaTiO3 nanoparticles were dried in an oven at 80°C for 24 hours. The reflux and particle retrieving processes were similar as in the surface functionalisation with 3-GPS. 3-GPS was then applied to BaTiO3 nanoparticles to improve the

processability and filler dispersion in nanocomposites; the solution of 1 wt.% of 3-GPS with respect to BaTiO3 was prepared. 150mL aqueous solution of ethanol and deionized water (9:1) was firstly mixed in a beaker. Adding the acetic acid drops using a pipette and stir vigorously after each drop until the pH value of 3.5-4 measured by a METTLER TOLEDO pH meter was reached, stirred vigorously again for 3mins to form a clear solution. The low pH values of the solution facilitate the silane functionalisation process [24]. After the addition of the 0.1g 3-GPS solution to the acidified solution using a pipette, the mixture was left in an ultrasonic bath for 30mins to form a homogenous solution. 10g hydroxylated BaTiO3 powders was then added to the silane solution, and mixed under ultrasonic bath for 10mins for better filler wetting. Finally, the mixture was refluxed at the boiling temperature of ethanol, 78°C [25], at 100 rpm using a mechanical stirrer for six hours using a silicone oil bath over a hotplate. After refluxing, the BaTiO3 was washed three times with deionized water and retrieved using centrifugation at 4500 rpm. The silane treated BaTiO3 (Si-BaTiO3) powders were dried at 110°C for 24 hours to avoid any condensation of silanol groups at the surface. In the end, the powders were crushed in a mortar and pestle for the nanocomposites preparation. The size distribution of Si-BaTiO3 particles was analysed in its epoxy nanocomposite form.

The epoxy nanocomposite fabrication process including Si-BaTiO3 functionalisation is schematically illustrated in Figure 2. The epoxy resin nanosuspension with 1, 5, 10, 15 wt.% Si-BaTiO3 nanoparticles and 5, 10, 15 wt.% untreated BaTiO3 nanoparticles are were prepared as follows: Firstly, the weighed amount of BaTiO3 powders was added to ethanol and sonicated with an ice water bath for 2 min with a 10s pulse to form a homogenous solution. Then a weighed amount of epoxy and the previous mixed solution were blended in a beaker using a mechanical stirrer at 300 rpm and 80°C overnight under the fume hood to gradually remove the ethanol without precipitation of the particles. The mixture was weighed before and after the previous step to ensure the complete removal of ethanol. The curing agent was then added to the mixture with a weight ratio recommended by the company and stirred for a further 3mins. Finally, the mixture was placed in the vacuum oven at 30°C for 1 hour to remove bubbles at 29 inHg and achieve complete removal of ethanol. The whole mixture was poured into a mould made of two pieces of glass clamped with a 3 mm silicone gasket in-between. A uniform thickness of each sample was achieved with the assistance of this type of glass mould. They were then cured in the oven for 8 hours at 80°C as prescribed by the manufacturer, then cooled down to room temperature. The final samples were of size 160×140×3 mm3, and cut to different sizes using a precision cut-off machine BRILLANT 220.

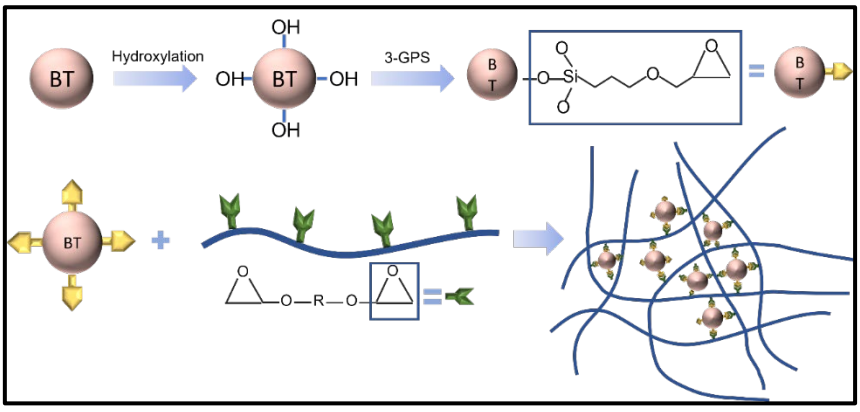

Figure 2. Schematic illustration of the hydroxylation and silane functionalisation process for the BaTiO3 nanoparticles.

3. In-situ Field-induced Strain Measurements

The microwave field was selected to be the external stimulator as BaTiO3 exhibit a peak in a dielectric loss at the microwave frequency range. Most importantly, the design of the experiment becomes more feasible with remote stimulation from the microwave field owing to the spacious cavity. The mechanical strain evolution in the nanocomposite was investigated under a microwave field within a temperature-controlled microwave cavity Panasonic NN-SF464MBPQ running at 2.45 GHz and cavity size of 354×338×230 mm3. In contrast with the conventional one, this oven, equipped with inverter technology, has a circuit board that replaces the transformer, hence the output power can be adjusted linearly by varying the pulse width to ensure a more precise and continuous microwave exposure [99]. The unique flat-bed design of this model is equipped with a stationary ceramic plate that allowed more space to place the sample and its holder.

The strain field introduced by the BaTiO3 nanoparticles to the surrounding epoxy, activated by microwave field, was studied by real-time strain measurements on the surface of the nanocomposite samples with the incorporation of Fibre optic sensors utilising fibre Bragg gratings (FBG) technique. The sensors were placed apart in equal distance from one another within a 90mm straight line. This is theoretically aligned with the microwave's half wavelength (~60mm) as also was experimentally observed during real-time temperature measurements. The sensors were located to ensure overlapping with at least three nodes and antinodes of the microwave cycle. The FBG sensors were fabricated by a periodic intense laser light applied onto the core of an optic fibre. The laser light exposure introduced a permanent increase in the refractive index of the fibre's core and a fixed modulation was created subsequently. Each FBG was approx. five mm long with a grating period of one micron. Two arrays with three FBGs for each sample were fabricated. FBG arrays were then adhesively bonded to the surface of two geometrically identical 135×10×3 mm3 samples made of Si-BaTiO3 epoxy nanocomposites. The strain array was bonded to the surface by adhesives at the FBG regions while the temperature array is firstly packaged into a capillary glass tube, and then bonded parallel to the strain array. The arrays were placed at the same location with the same distance in-between. The strain experienced by the samples was transferred to the FBG sensors, and the measurements were also affected by the temperature. Therefore, the temperature array only measured the temperature change, and compensated the strain measurements accordingly.

A preliminary test via a FLIR One Pro LT Thermal Camera was carried out to inspect the temperature change in different samples under different microwave power levels. Samples were placed at a designed location as shown in Figure 3. The exposure time was then carefully selected based on the heating profiles of each sample to control the temperature of samples well below Tg during the exposure to avoid any interference in strain measurements from the post-cure shrinkage. The sample was clamped on one end by a designed sample holder made of polytetrafluoroethylene (PTFE) to ensure minimum interaction with the microwave field owing to its extremely low dielectric loss. The size and location of the load inside the cavity were two primary factors that affect the microwave field distribution [26]. To control the microwave field distribution, the sample and the holder were placed at the designed location

shown in the figure, for all tests. The power level of 100W and 440W were initially selected to avoid temperature surges in samples within a short period of time. Exposure time was set to be 650s for 100W and 148s for 440W to limit the temperature below Tg (80°C) based on the preliminary results obtained by the thermal camera.

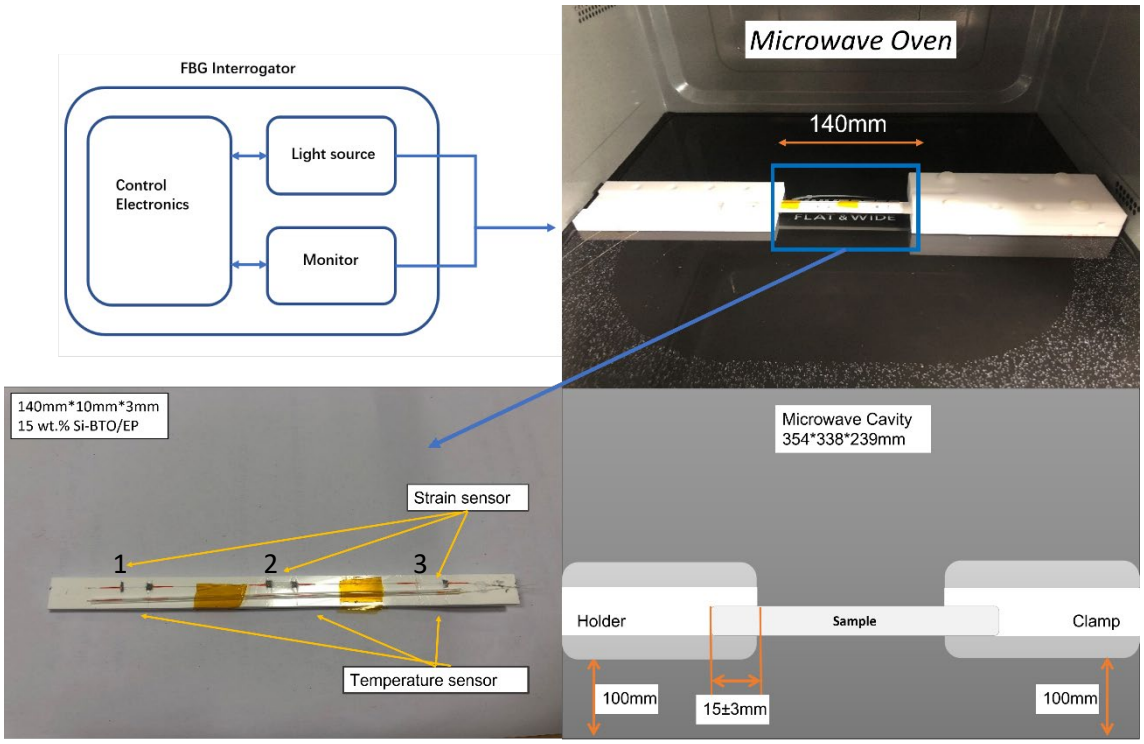

Figure 3. Illustration of the sample of epoxy nanocomposite with BaTiO3 on the PTFE holder in the microwave oven with surface bonded FBG arrays connected to an interrogator.

Neat epoxy, BaTiO3 nanoparticles, and adhesive used for bonding FBGs possess different thermal expansion coefficients (CTE) and microwave heating patterns. Microwave field interaction with the neat epoxy and adhesive have been investigated, thereafter. Two arrays with five FBGs of five mm long and one micron grating period were fabricated for each test. First, the adhesive response under microwave radiation was studied by two arrays of FBGs adhesively bonded to the surface of a PTFE block. It is assumed that measured strain and temperature change are solely due to the microwave heating of adhesive as PTFE has neglectable thermal response (temperature rise) under the microwave. The PTFE block is placed in the microwave oven at the designed location to locate the first FBG sensor on the left end at the same location as the one in the previous exposure on the nanocomposites. The tests have been performed under 100W for 650s and 440W for 110s. Data was recorded on the interrogator 10s prior to the microwave exposure for each run to ensure no data is missing after the microwave starts. The effect of neat epoxy with the FBG sensors bonded to its surface was investigated as a controlled group to the test of 15 wt.% nanocomposites at 10 W for 600s and 440W for 60s. Neat epoxy sample geometrically identical with 15 wt.% nanocomposites in the nanocomposite's exposure test was placed in the designed location with surface-bonded arrays of FBGs. The whole measurements from adhesive and the neat epoxy were compared with the results from the previously performed test on the

nanocomposites for better distinguishing the BaTiO3-epoxy nanocomposite's response to the microwave exposure.

4. Results and Discussion

Labelling for strain and temperature FBG arrays is illustrated in Figure 3. Field-induced strains in the nanocomposites with 15 wt.% BaTiO3 (the highest wt.% examined) has been investigated within a microwave exposure at 100W and 440W (Figure 5 and Figure 6, respectively). The evolution of strain and temperature have been measured in situ by the two arrays; one array measures the strain while the other one measures the temperature. Sudden drastic fluctuations and absent data presented in the figures are due to Bragg wavelengths moving into adjacent spectral windows that were set up on the sensor interrogator.

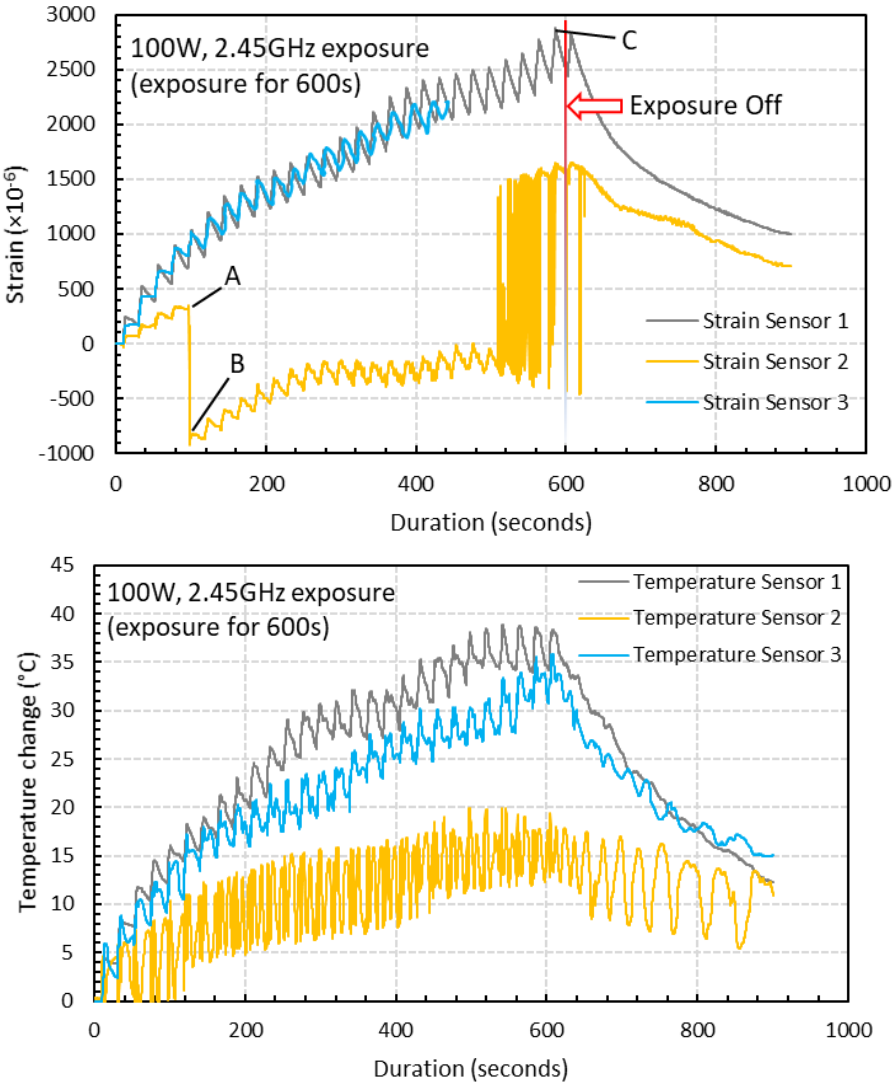

Figure 5. Strain and temperature change measurements of 15 wt.% silane-treated BaTiO3/Epoxy samples under 100W for 600s.

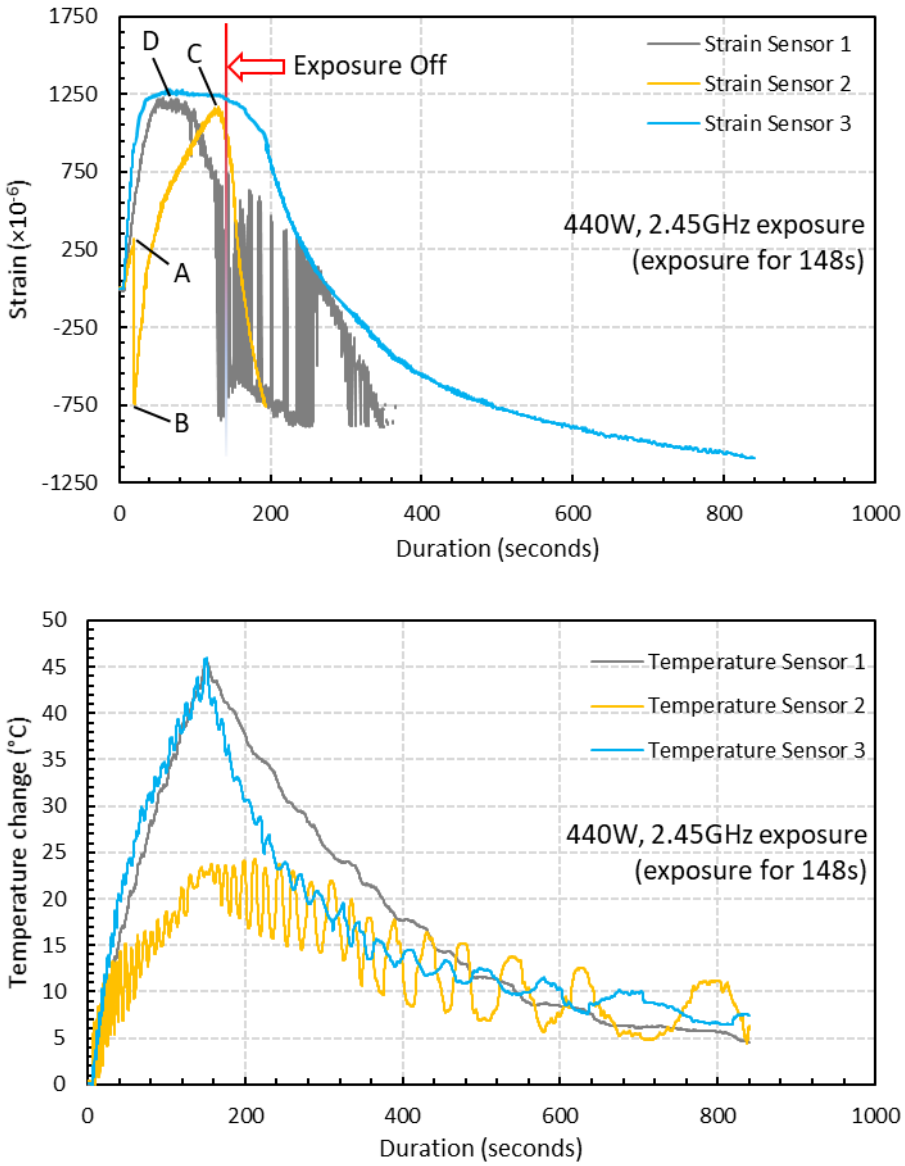

Figure 6. Strain and temperature change measurements of 15 wt.% silane-treated BaTiO3/Epoxy samples under 440W for 148s.

The strain and temperature data exhibit a general increasing trend with the exposure. They drop gradually, immediately, after the microwave stopped. The temperature appeared to be higher at both ends of the specimen (sensor 1 and 3, located left and right respectively) compared to the middle (sensor 2), which is in accordance with the 'hot spot' theory due to microwave nonuniformity. Sensors 1 and 3 data also follows more similar temperature increasing trend (magnitude and rate).

Under the 100W and 440W, the strain measured at the beginning of the microwave radiation in strain sensors 1 and 3 have similar trends of increasing as predicted when the temperature sensors 1 and 3 measurements have close gradients, having higher temperatures than that measured by sensor 2. A sudden drop in the strain measurements of the middle sensors (strain 2) can be observed in both cases soon after the initial surge, labelled as A-B. It instantaneously alters the strains by nearly identical 1162 and 1008 micro-strains (difference between A and B)

under 100W and 440W, respectively. Such decline in the strain measurements is the evidence of attributed to an immediate development of a compressive strain in response to the microwave exposure, as hypothesised. Note that sensor 2 temperature is the lowest amongst the three sensors, in which the thermally induced strain is negligible. Such phenomenon could not be associated with the temperature rise since the temperature change is approximately 12°C and 5.7°C from room temperature 19°C when the sudden drop occurs at point A, which is remarkably lower than 170°C when post-curing shrinkage is introduced as indicated by the exothermic peak in our DSC measurements, and lower than the Tg to have any detrimental effect. Moreover, it is observed that unloading the specimen from the 440W exposure results in a residual compressive strain in all sensors' locations. This occurs after the high non-linear variation of strains in the case of 440W, unlike the linear strain behaviour under 100W. This is analogous to mechanical field introduction in which unloading an elastic-plastic specimen beyond its elastic regime under tensile loading may introduce a compressive residual strain distribution depending on the hardening behaviour (i.e. kinematic or isotropic). The strain and temperature measurements as a function of energy absorbed in Joules are presented below, under 100W and 440W.

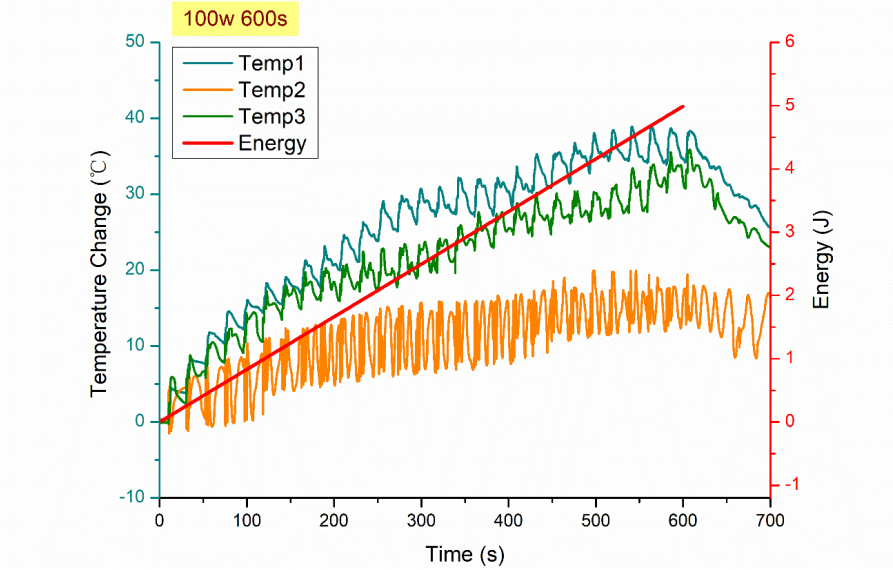

Figure 7. Temperature change measurements (micro-strain) by FBG sensors (left), and energy absorbed (right) versus time (s) under 100W.

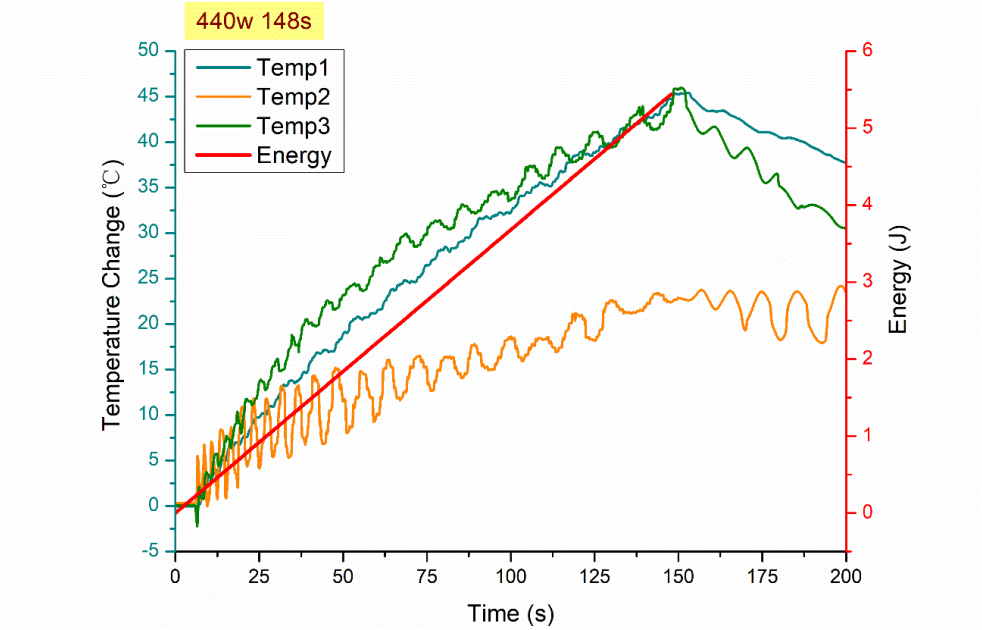

Figure 8. Temperature change measurements (micro-strain) by FBG sensors (left), and energy absorbed (right) versus time (s) under 440W.

It could be observed that, the energy absorption rate is close to the rate of temperature rise in the FBG sensors. At the beginning of the microwave exposure, the temperature rise exhibits a similar rate compared with the energy absorption rate. As the exposure time increases, the temperature rise becomes significantly slower. The 'hot spot' theory due to the non-uniformity of microwave fields is proposed to be the possible explanation of this phenomenon as described formerly.

5. Conclusion

The quantitative research on microwave field-nanocomposite interaction was conducted to study the ferroelectric materials' response in high-performance (rigid) epoxy composite that offers reversible microwave activated electro-strains introduced by a second dielectric phase (BaTiO3). The data presented a pioneering investigation as no investigations have been reported, thus far, on the micromechanical (extrinsic) strain response of rigidly constrained ferroelectric materials in polymer under external electromagnetic fields. FBG sensors-based technique was employed, in-situ with the microwave exposure, for real-time monitoring of the strain and temperature response of the nanocomposite subjected to a 2.45GHz microwave field at controlled exposure power and energy, followed by newly developed theoretical constitutive equations underpinning field-material interactions.

A time-dependent strain field is introduced, proportional to the exposure time/energy, in the multi-domain BaTiO3 nanoparticles under the stimulation of a microwave field, linearly under 100W and non-linearly under 440W. A sudden drop in micro-strain data by the value of approx. 1000 compressive micro-strains was observed in the BaTiO3-epoxy composites at the beginning phase of the exposure under the different exposure powers examined, a potential for active toughening. Such phenomenon has not been reported thus far in the existing literature, and is under investigation of our research group.

6. Acknowledgment

The authors would like to acknowledge the grants received for this research from the UK Engineering & Physical Sciences Research Council (EPSRC), Ref. EP/R016828/1 (Self-tuning Fibre-Reinforced Polymer Adaptive Nanocomposite, STRAINcomp) and EP/R513027/1 (Study of Microstructure of Dielectric Polymer Nanocomposites subjected to Electromagnetic Field for Development of Self-toughening Lightweight Composites), and Foundation for Polish Science (FNP) under Grant Number First TEAM/2016-1/7, co-funded by the European Regional Development Fund.

References

[1] Ozdemir, N.G., et al., Toughening of carbon fibre reinforced polymer composites with rubber nanoparticles for advanced industrial applications. Express Polymer Letters, 2016. 10(5): p. 394-407.
[2] Cantwell, W.J. and J. Morton, The impact resistance of composite materials — a review. Composites, 1991. 22(5): p. 347-362.
[3] Yazdani Nezhad, H., et al., Numerical analysis of low-velocity rigid-body impact response of composite panels. International Journal of Crashworthiness, 2015. 20(1): p. 27-43.
[4] Camanho, P.P., et al., Prediction of in situ strengths and matrix cracking in composites under transverse tension and in-plane shear. Composites Part A: Applied Science and Manufacturing, 2006. 37(2): p. 165-176.
[5] Hernandez, T.P.A., A.R. Mills, and H. Yazdani Nezhad, Shear driven deformation and damage mechanisms in High-performance carbon Fibre-reinforced thermoplastic and toughened thermoset composites subjected to high strain loading. Composite Structures, 2021. 261: p. 113289.
[6] Alshammari, B.A., et al., Comprehensive Review of the Properties and Modifications of Carbon Fiber-Reinforced Thermoplastic Composites. Polymers, 2021. 13(15): p. 2474.
[7] Ratna, D. and A.K. Banthia, Rubber toughened epoxy. Macromolecular Research, 2004. 12(1): p. 11-21.
[8] Ma, J., et al., Effect of inorganic nanoparticles on mechanical property, fracture toughness and toughening mechanism of two epoxy systems. Polymer, 2008. 49(16): p. 3510-3523.
[9] Thostenson, E.T. and T.-W. Chou, Processing-structure-multi-functional property relationship in carbon nanotube/epoxy composites. Carbon, 2006. 44(14): p. 3022-3029.
[10] Eqra, R., K. Janghorban, and H. Daneshmanesh, Mechanical properties and toughening mechanisms of epoxy/graphene nanocomposites. Journal of Polymer Engineering, 2015. 35(3): p. 257-266.
[11] Liu, T., et al., Morphology and fracture behavior of intercalated epoxy/clay nanocomposites. Journal of Applied Polymer Science, 2004. 94(3): p. 1236-1244.
[12] An, Q., A.N. Rider, and E.T. Thostenson, Hierarchical Composite Structures Prepared by Electrophoretic Deposition of Carbon Nanotubes onto Glass Fibers. ACS Applied Materials & Interfaces, 2013. 5(6): p. 2022-2032.
[13] Yazdani Nezhad, H., and Thaku, V.K., Effect of morphological changes due to increasing carbon nanoparticles content on the quasi-static mechanical response of epoxy resin. Polymers, 2018. 10(10): 1106.
[14] An, D., et al. Ultra-thin electrospun nanofibers for development of damage-tolerant composite laminates. Materials Today Chemistry, 2019. 14: 100202.

[15]Bregar, T., et al. Carbon nanotube embedded adhesives for real-time monitoring of adhesion failure in high performance adhesively bonded joints. Scientific Reports, 2020. 10(1): p.1-20
[16]Khaleque, T., et al. Tailoring of thermo-mechanical properties of hybrid composite-metal bonded joints. Polymers, 2021. 13(2): 170.
[17]Awaja, F., et al., Cracks, microcracks and fracture in polymer structures: Formation, detection, autonomic repair. Progress in Materials Science, 2016. 83: p. 536-573.
[18]Damjanovic, D., Contributions to the piezoelectric effect in ferroelectric single crystals and ceramics. Journal of the American Ceramic Society, 2005. 88(10): p. 2663-2676.
[19]Jones J.L., N.J.C., Pramanick A., Daniels J.E, Time-Resolved, Electric-Field-Induced Domain Switching and Strain in Ferroelectric Ceramics and Crystals. In: Eckold G., Schober H., Nagler S. (eds) Studying Kinetics with Neutrons. Springer Series in Solid-State Sciences, vol 161. Springer, Berlin, Heidelberg. https://doi.org/10.1007/978-3-642-03309-4_6. 2009.
[20]Gao, J.H., et al., Recent Progress on BaTiO3-Based Piezoelectric Ceramics for Actuator Applications. Actuators, 2017. 6(3): p. 20.
[21]Shen, Z.-Y. and J.-F. Li, Enhancement of piezoelectric constant d33 in BaTiO3 ceramics due to nano-domain structure. Journal of the Ceramic Society of Japan, 2010. 118(1382): p. 940-943.
[22]Hsiang, H.I. and F.S. Yen, Effect of crystallite size on the ferroelectric domain growth of ultrafine BaTiO3 powders. Journal of the American Ceramic Society, 1996. 79(4): p. 1053-1060.
[23]Polotai, A.V., A.V. Ragulya, and C.A. Randall, Preparation and Size Effect in Pure Nanocrystalline Barium Titanate Ceramics. Ferroelectrics, 2003. 288(1): p. 93-102.
[24]Zhou, T., et al., Improving Dielectric Properties of BaTiO3/Ferroelectric Polymer Composites by Employing Surface Hydroxylated BaTiO3 Nanoparticles. Acs Applied Materials & Interfaces, 2011. 3(7): p. 2184-2188.
[25]Ambrożewicz, D., et al., Fluoroalkylsilane versus Alkylsilane as Hydrophobic Agents for Silica and Silicates. Journal of Nanomaterials, 2013. 2013: p. 631938.
[26]UK, F.S. https://www.fishersci.co.uk/shop/products/ethanol-absolute-200-proof-molecular-biology-grade-fisher-bioreagents-5/16606002. 2021.
[27]Bansal, P., E. Vineyard, and O. Abdelaziz, Advances in household appliances- A review. Applied Thermal Engineering, 2011. 31(17): p. 3748-3760.

